Verification of the Beam Phase Control System Topology for FAIR by Beam Experiments

Christoph Julien Wegmann, Dieter Lens, Bernhard Zipfel, Christoph Reinwald, and Harald Klingbeil

***Abstract*—Beam phase control loops have become an important sub-system of the low-level radio frequency (LLRF) systems of ion synchrotrons. A wide range of different implementations exists today. The LLRF system at the GSI Helmholtzzentrum für Schwerionenforschung (GSI)/Facility for Antiproton and Ion Research in Europe (FAIR) was designed with the particular goals of modularity, flexibility, scalability, and user-friendly diagnostics possibilities. Based on these requirements, a system focused on the time-domain manipulation of all RF and beam signals was developed. This contribution presents the beam phase control system and demonstrates its effectiveness. The special attention is paid to the operation during the acceleration ramp. Results of two independent beam experiments are presented: one focused on examining the control loop behavior and one applying the system in a practical setting. In both cases, the GSI/FAIR beam phase control system successfully dampens longitudinal dipole mode bunch oscillations. Its performance and behavior matches previous analyses.**

***Index Terms*—Beam phase control, ion accelerators, low-level RF, synchrotrons.**

I. Introduction

ION synchrotrons in the low-energy regime generally span a large frequency range. Especially, the smaller rings, used, for example, for medical applications, can show a relative frequency change by a factor of 7. Examples can be found in the synchrotron at the Heidelberger Ion Beam Therapy Center (HIT) with a circumference of 65 m and a frequency range of $f_{\mathrm{RF}} = 1, \ldots, 7$ MHz at $h = 2$ [1], [2], [3], the MedAustron synchrotron with a circumference of 77 m and a frequency range of $f_{\mathrm{RF}} = 0.47, \ldots, 3.26$ MHz at $h = 1$ [4], [5], [6] or the low energy ion ring (LEIR) at European Organization for Nuclear Research (CERN) with a circumference of 78.5 m and a frequency range of $f_{\mathrm{RF}} = 720$ kHz$, \ldots, 2.84$ MHz$/f_{\mathrm{RF}} = 1.08, \ldots, 4.26$ MHz at $h = 2/h = 3$ [7], [8], [9], [10], [11], [12], [13], [14]. But also the larger ion rings (especially booster synchrotrons) can feature substantial changes in frequency during acceleration. An overview of such accelerators is given in Table I.

Received 4 November 2025; revised 19 March 2026; accepted 19 April 2026. Date of publication 23 April 2026; date of current version 19 May 2026. *(Corresponding author: Christoph Julien Wegmann.)*

Christoph Julien Wegmann and Christoph Reinwald are with the Accelerator Technology Group, Technical University of Darmstadt (TU Darmstadt), 64289 Darmstadt, Germany (e-mail: julien.wegmann@tu-darmstadt.de; christoph_juergen.reinwald@tu-darmstadt.de).

Dieter Lens and Bernhard Zipfel are with the Ring RF Systems Department, GSI Helmholtzzentrum für Schwerionenforschung GmbH (GSI), 64291 Darmstadt, Germany (e-mail: D.E.M.Lens@gsi.de; B.Zipfel@gsi.de).

Harald Klingbeil is with the Accelerator Technology Group, TU Darmstadt, 64289 Darmstadt, Germany, and also with the Ring RF Systems Department, GSI, 64291 Darmstadt, Germany (e-mail: klingbeil@temf.tu-darmstadt.de).

Color versions of one or more figures in this article are available at https://doi.org/10.1109/TNS.2026.3687074.

Digital Object Identifier 10.1109/TNS.2026.3687074

Beam phase control loops have become an important sub-system of the low-level radio frequency (LLRF) systems of ion synchrotrons (see [32], [33], [34], [35], [36], [37] for cavity control techniques). While some facilities do not use local control loops [19], a combination of local and central control loops is used in others: Local control loops counteract beam loading [21], [31], [38] or account for differences between the individual RF cavities, e.g., due to the transmission delay or ring position [38]. The beam phase control, on the other hand, dampens bunch oscillations (see, for example, the results presented in [22]), leading to a cascaded structure of phase control loops. Special care must be taken that resulting shifts of the cavity voltage are identically realized by all RF stations [39], [40] and for all harmonics [21], [22], [23], [40].

The implementation of the control systems varies for different facilities based on their specific focus, requirements, and restrictions. Some aspects of the design of the current LLRF systems at Japan Proton Accelerator Research Complex (J-PARC), Brookhaven National Laboratory (BNL), Fermi National Accelerator Laboratory (Fermilab), and CERN will be highlighted here. At BNL and CERN, the discussed control systems are used in a similar fashion for a group of accelerators [13], [39], [40].

As described in [27] and [31], the primary goals of the LLRF upgrade for the CERN ion synchrotrons are the expansion of its operational capabilities and the simplification of maintenance and operation. For example, it resulted in switching from a variable to a constant clock frequency [12], [13], [38], [40] and the integration of diagnostics to measure the control loop behavior [38]. A similar idea of including built-in identification tools directly in the LLRF system can also be found at Fermilab [19]. Both, in the Rapid Cycling Synchrotron (RCS) at J-PARC and the Proton Synchrotron Booster (PS Booster) at CERN, broadband MA-loaded cavities are used, whereby each individual cavity generates multiple harmonic components simultaneously [21], [23], [40], [41]. Furthermore, at both facilities a similar implementation topology is employed, in which manipulations of the control loops from measured RF gap voltage signals to RF power amplifier (driver) inputs are performed digitally separated by harmonic components [21], [22], [23], [38], [40]. For the PS booster, this is achieved using a digital multi-harmonic local oscillator to which the revolution frequency is supplied [38], [40].

TABLE I

COMPARISON OF SOME LARGE-SCALE (>150 METERS) ION SYNCHROTRONS WITH A LARGE FREQUENCY SPAN

Facility Synchrotron	GSI/FAIR SIS18	Fermilab Booster	J-PARC RCS	BNL Booster	CERN PS Booster
Accelerated Elements	H to U	H [19], [20]	H [21], [22]	H to Au [24]	H [13], [27], prev. also e.g. O, Pb [28], [29], [30]
Circumference	216 m [15], [16]	474 m [19]	348.3 m [21], [22], [23]	201.8 m [24]	157 m [30]
RF Frequency Span of Main Harmonic	400 kHz ...2.8 MHz / 800 kHz ...5.6 MHz [16], [17]	44.7 MHz...52.8 MHz [19], [20]	1.22 MHz...1.67 MHz [21], [22], [23]	e.g. 398 kHz...3.84 MHz (Au, 2010) [25]	1.0 MHz...1.8 MHz [31]
Main Harmonic (Example)	$h = 2$ / $h = 4$ [16]	$h = 84$ [19], [20]	$h = 2$ [21], [22]	$h = 6$ (Au, 2010) [25]	$h = 1$ [31]
Acceleration Time	150 ms [18]	35 ms [19]	20 ms [21], [22]	80 ms (Au) [25], [26]	500 ms [13], [27]

Alternatively, in the RCS LLRF system the revolution frequency is integrated to phase values which are multiplied by the respective harmonic number [21], [23]. Each cavity (or group of cavities) is controlled by its dedicated digital module. Those communicate with central modules implementing the shared functionalities such as the beam phase control [13], [21], [31], [40]. This is similar to the implementation at BNL [39]. On the other hand, the Fermilab Booster control system is based on a central module which directly generates the cavity driver signals [19]. The beam phase control at BNL is operated in parallel to a bunch-by-bunch phase feedback with a dedicated kicker cavity by separately processing average and individual phase errors of the bunches [39]. Of course, other (local cavity) control loops such as fast RF feedback [31], [33], RF feedforward [21], [23], [33], [38], [42], [43], cavity tune control [39], or radial position control [19], [44], [45], [46] are or have been (as mentioned in [21] and [22]) an essential part in many LLRF systems but are outside the scope of this contribution.

The Facility for Antiproton and Ion Research in Europe (FAIR) LLRF system that is also used for the existing GSI synchrotrons was developed with the aims of high modularity, flexibility, scalability, and user-friendly diagnostic possibilities. It is based on a delay-compensated distribution of clock signals and a synchronous synthesis of frequency-variable reference RF signals in different supply rooms [62]. Therefore, all signals can be analyzed by standard oscilloscopes. The above-mentioned features of the beam phase control subsystem are implemented by a nested control-loop combining the beam-phase control itself with the local cavity synchronization systems in a modular way.

Sections II–IV are structured as follows. In Section II, an overview of the GSI/FAIR beam phase control system is given. The special attention is paid to the topology of interaction between cavity and beam phase control loops as well as the steps taken to operate the beam phase control during acceleration. The performance of the beam phase control on the ramp is discussed based on the measurement data from two beam experiments in Section III. Finally, Section IV gives a summary of the key results. A part of the shown measurements had previously been presented in a brief technical overview [47]. This contribution provides a more detailed discussion of the underlying control systems and their design, further results as well as an in-depth analysis.

II. GSI/FAIR CONTROL SYSTEM TOPOLOGY AND OPERATION PRINCIPLE

The following overview of the GSI/FAIR beam phase control system will focus primarily on new and unique aspects of the control topology and implementation. The presented system was operated during the machine experiments described in Section III.

A. Beam Phase Control System

Fig. 1 shows a top-level block diagram of the GSI/FAIR beam phase control system used in the experiments presented in Section III. Components related to, e.g., amplitude control loops as well as calibration/feedforward modules are omitted for the sake of clarity.

In this specific scenario, two RF cavities were used running at the same harmonic number, but the chosen topology allows an arbitrary number of cavities and also multi-harmonic operation [48], [49], [62]. Each cavity has its local direct digital synthesis (DDS) module, called cavity DDS. The cavity DDS realizes the required RF frequency ramp (at the required harmonic number) and runs on its local (asynchronous) clock. The output of the cavity DDS is used to generate (via the amplitude control loop) the driver amplifier input signal. Its output drives a tetrode power amplifier in the cavity, leading to the RF voltage at the gap. For the cavity (phase) synchronization, the gap voltage is measured and fed back to a local synchronization system that also receives a corresponding reference signal at the same harmonic number. This reference signal is called group DDS signal [48], [62] and is produced by DDS modules that are provided with campus-wide synchronous clocks. The synchronization system is based on digital signal processing technology [50]. It supplies its cavity DDS with a frequency correction Δf_{corr} such that the cavity phase follows the target phase provided by the central control system.

In order to dampen coherent bunch oscillations, this local synchronization control is embedded in an additional beam phase control loop. To this end, the beam phase is measured with respect to the group DDS signal by processing the beam signal picked up by a fast current transformer (FCT) with a beam phase control DSP (BPC DSP). In addition, the BPC DSP realizes a filter system to extract information about bunch oscillations and the control algorithm calculations. This filter setup is discussed more closely in Section II-B. In accordance

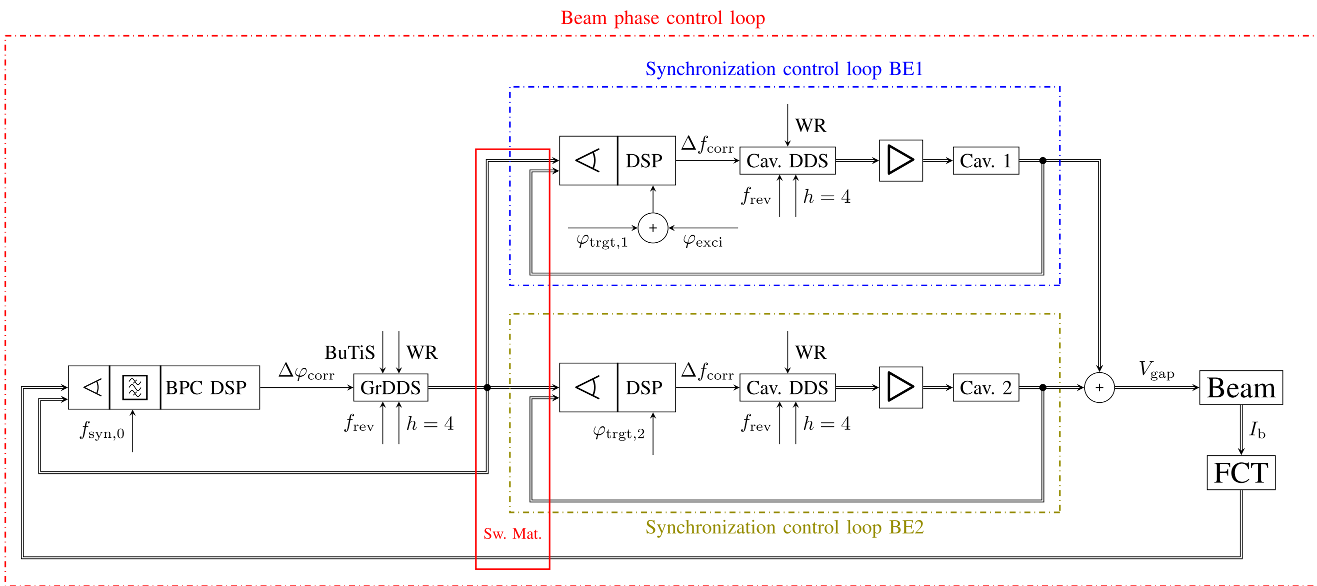

Fig. 1. Schematic of the GSI/FAIR beam phase control system. RF signals are drawn as double-lined arrows.

with dampening detected dipole mode bunch oscillations [32], [52], [53], the BPC DSP supplies the group DDS module with a phase correction $\Delta\varphi_{\text{corr}}$. The two RF signals that are fed to the phase detection of the BPC DSP are routed through a switch matrix (Sw. Mat.) [47], allowing an automatic selection of the group DDS signal with the correct harmonic number. In principle, the switch matrix also allows to select other signals as reference for the beam phase control (such as the voltage of one particular cavity, or a group DDS signal that is not phase-shifted), but this is currently not planned. All RF signals arriving at the switch matrix are delay-compensated.

Some particular features of the GSI/FAIR beam phase control system should explicitly be highlighted. First, the RF signal of each cavity system is individually synthesized locally by its cavity DDS, which is locked by the cavity synchronization system to a group DDS signal. Since the RF systems are distributed among several supply areas, phase-synchronous group DDS signals are generated in several locations. For this purpose, the bunchphase timing system (BuTiS) [54], [55] and the white rabbit (WR) [56], [57], [58], [59] infrastructure are utilized [60], [61] such that synchronous signals can be generated at different locations without the need for a central distribution of variable-frequency RF signals (see also [48], [62]). Overall, an accuracy of $\pm 3^\circ$ for the phase of the gap voltage under dynamic conditions is required [48], [63]. This value includes all influences of the entire signal chain and is primarily determined by the signal processing hardware and the accuracy of a phase calibration procedure [48], [63]. For most RF systems of SIS18, this has already been achieved (see [64]) including errors of the GrDDS signals smaller than $\pm 0.5^\circ$ (at $h = 1$) [48]. Second, the structure of the BPC DSP controlling the group DDS signal, which acts as the common reference for each individual local synchronization loop, leads to a cascaded control system. A shift in the group DDS signal due to activation of the beam phase control is transferred to the cavity voltages through the synchronization loop of each cavity. Third, in contrast to the systems discussed in Section I, the GSI/FAIR LLRF system is not comprised of large digital modules but instead built up from a modular toolbox of components. Through the use of clearly defined interfaces, standardized LLRF modules can be used for different purposes. For example, the same type of DSP systems is used for cavity synchronization and beam phase control. In this way, a solution is found combining the ease of maintenance, flexibility, and performance of digital components with extensive capabilities for time-domain diagnostics and overall scalability.

An extension to more than two cavities is straightforward (and has already been realized). The system is also suitable for multi-harmonic operation [49]. All components in Fig. 1 drawn to the right of the driver amplifiers are located in the accelerator tunnel, whereas everything to the left, as well as the driver amplifiers themselves are located in the RF supply areas. More details can be found, for example, in [50], [51], and [62].

B. Measurement of Beam Oscillations

Due to its importance to the beam phase control loop, the method for measuring bunch oscillations using the FCT signal in the BPC DSP will be examined in more detail. The initial approach was presented in [51]. Therefore, the following description will focus on extensions necessary to operate the BPC on the ramp.

After the analog mixing and filtering stage, the signal is digitized, and the phase difference between the group DDS and beam signal is calculated [50]. To dampen dipole modes, a 90° phase shift at the synchrotron frequency is required [37] while slowly varying phase displacements—like the synchronous bunch phase during acceleration—must remain unaffected. In addition, the feedback shall not excite higher order modes or increase unwanted frequency components, since in ion machines the emittance of the beam is sensitive to

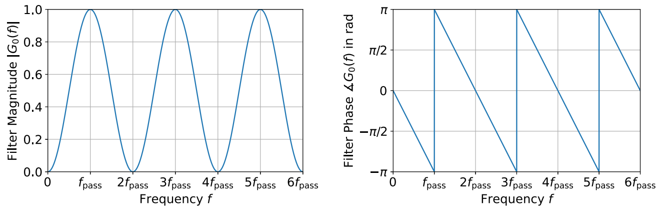

Fig. 2. Transfer function of the three-tap FIR filter. Magnitude (left). Phase (right).

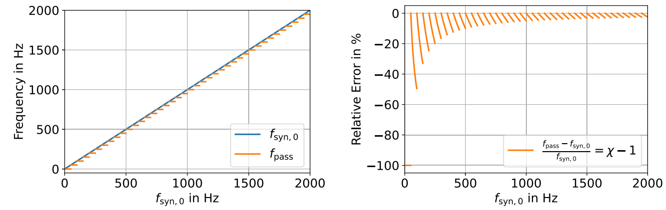

Fig. 3. Comparison between the synchrotron frequency and the filter center frequency f_{pass} under the presented scheme. Selected values for f_{pass} (left). Relative error (right).

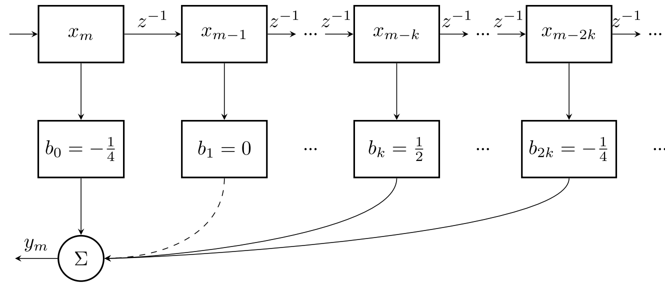

Fig. 4. Data flow of the three-tap FIR filter. For efficiency, only contributions with $b_k \neq 0$ are considered in the calculation of the sum.

noise-induced excitation due to the lack of natural damping from synchrotron radiation [37], [65]. These requirements are realized by processing the digital data samples x_i using a 3-tap finite impulse response (FIR) filter [51]

$$y_m = \sum_{l=0}^{l_{\max}=2k} b_l \cdot x_{m-l} = -\frac{1}{4}x_m + \frac{1}{2}x_{m-k} - \frac{1}{4}x_{m-2k}. \quad (1)$$

Only the filter taps corresponding to $l \in \{0, k, 2k\}$ with $l_{\max} = 2k$ are unequal to 0. The transfer function of this filter is

$$G_0(j\omega) = \frac{Y(j\omega)}{X(j\omega)} = \frac{1}{2}e^{-jk\omega T_s}\left[1 - \cos(k\omega T_s)\right] \quad (2)$$

with the sampling period of the DSP system being

$$T_s = \frac{1}{f_s} = \frac{1}{310\ \text{kHz}}. \quad (3)$$

This transfer function is drawn in Fig. 2. The first maximum of the magnitude characteristic is located at

$$f_{\text{pass}} = \frac{1}{2kT_s} \quad \Leftrightarrow \quad k = \frac{1}{2T_s f_{\text{pass}}} \quad (4)$$

meaning that the parameter k selects which of the samples are to be processed via the coefficients b_i as specified in (1). Depending on this setting, the frequency component at f_{pass} is extracted with $\measuredangle G_0(j2\pi f_{\text{pass}}) = 180°$. Introducing an integration

$$z_m = a z_{m-1} + y_m \quad (5)$$

with a slightly smaller than 1 to prevent a wind-up, leads to the overall transfer function for $f \ll f_s$ being approximately

$$G_1(j\omega) = \frac{Z(j\omega)}{X(j\omega)} = \frac{G_0(j\omega)}{j\omega T_s}. \quad (6)$$

In the machine experiments presented in Section III, the value $a = 0.99$ is used. The integration additionally reduces the phase by 90°, meaning that the required phase of $\measuredangle G_1(j2\pi f_{\text{pass}}) = 90°$ needed to dampen bunch oscillations [37] is reached if k is selected so that f_{pass} approximates the frequency of this oscillation. Low-frequency noise—as well as slowly varying changes of the phase difference, for example, due to changes in the synchronous phase during acceleration—do not affect the control loop as they are suppressed by the FIR filter, while high-frequency noise is suppressed by the integration.

Since the synchrotron frequency changes during acceleration, so must also f_{pass}. This is achieved by preparing a table of filters between which the BPC DSP switches in real-time. The center frequency f_{pass} of each filter differs from that of the next one by a (configurable) value Δf. During acceleration, the index of the filter whose center frequency fits to the linear synchrotron frequency $f_{\text{syn},0}$ (which is calculated in advance) is determined as follows:

$$n_{\text{filt}} = \lfloor p_f \cdot f_{\text{syn},0} \rfloor \quad (7)$$

where $\lfloor \cdots \rfloor$ denotes the rounding by the floor function. The center frequency of this filter is then simply

$$f_{\text{pass}} = \Delta f \cdot n_{\text{filt}} = \Delta f \cdot \lfloor p_f \cdot f_{\text{syn},0} \rfloor. \quad (8)$$

With the standard configuration of $\Delta f = 50$ Hz and $p_f = 0.02$, a range of 0 Hz $\leq f_{\text{syn},0} \leq$ 6399 Hz is covered by a total of 128 filters. Fig. 3 visualizes the selected f_{pass} based on $f_{\text{syn},0}$. For a large synchrotron frequency, the filter center frequency yields a good approximation (even when switching between filters), whereas for smaller values, the relative error can increase due to the constant difference between the center frequency of adjacent filters Δf. An extension for using non-uniformly distributed filter ranges is in development. This would decrease Δf for smaller synchrotron frequencies so that the relative error between f_{pass} and $f_{\text{syn},0}$ does not become as large as in the current implementation. The effect of mismatches between synchrotron and filter center frequency was studied in [51] and is analyzed in Section III-C for operation on the ramp.

Dynamically switching between three-tap filters introduces the difficulty that each processed value y_i has to depend on the coefficients of only one respective filter. The scheme to achieve this is sketched in Fig. 4. During each cycle of the main clock, a new data point is included, all existing data values are propagated by one step, and the filter is fully evaluated. Therefore, a new valid output value of the filter is produced each main clock cycle even if the filter coefficients are exchanged in that cycle.

Each DSP system monitors both, frequency and amplitude values, which are calculated in real-time on an

FPGA [66], [67]. To prevent disturbances due to inaccurate readouts, phase values are declared to be invalid if the corresponding amplitude is below a configurable threshold (implemented as hysteresis to avoid repeated discarding of data, e.g., due to noise). The filter output is only processed if all stored phase values required for the currently active filter are valid.

If the filter center frequency is varied as $f_{\text{pass}} = \chi f_{\text{syn},0}$, the open-loop transfer function of the beam phase control can be written in analogy to [51] as follows:

$$G_{\text{open}}(\omega) = \frac{\frac{K}{\omega_{\text{syn},0}}}{2j\frac{\omega}{\omega_{\text{syn},0}}} e^{-j\frac{\pi}{\chi}\frac{\omega}{\omega_{\text{syn},0}}} \left[1 - \cos\left(\frac{\pi}{\chi}\frac{\omega}{\omega_{\text{syn},0}}\right)\right] \times \frac{\left(\frac{\omega}{\omega_{\text{syn},0}}\right)^2}{1 - \left(\frac{\omega}{\omega_{\text{syn},0}}\right)^2} e^{-j\omega_{\text{syn},0} T_{\text{D}} \frac{\omega}{\omega_{\text{syn},0}}} \tag{9}$$

$$K = K_{\text{p}} f_{\text{s}} K_{\text{scale}} > 0 \tag{10}$$

where T_{D} denotes the overall loop delay, K_{p} denotes the controller gain, and K_{scale} denotes the other scaling factors. It can be seen that the dynamic of the control loop relative to the synchrotron oscillation is constant if the loop gain is also varied as $K \propto f_{\text{syn},0}$ (under the reasonable assumption of $f_{\text{syn},0} T_{\text{D}} \ll 1$, see, e.g., also the stability analysis in [51, Appendix]). Previous analyses [49], [51] determined suitable values as follows:

$$\chi = \frac{f_{\text{pass}}}{f_{\text{syn},0}} = 1.0, \ldots, 1.1, \quad \frac{K}{\omega_{\text{syn},0}} = 0.35. \tag{11}$$

III. Results

Sections III-A–III-D present results obtained from operating the beam phase control in two independent experiments at the GSI heavy-ion synchrotron SIS18. A machine development experiment (MDE) was used to analyze the properties of the beam phase control system in detail, using dedicated RF manipulations (phase jumps) to excite dipole oscillations at lower beam intensities in a reproducible way. In a further experiment, a standard machine pattern was used, where dipole oscillations occurred at higher beam currents without RF manipulations, thus offering a realistic scenario comparable to standard beam operation. For experiment cycles using the beam phase control, the system was switched on before injection and remained active until after extraction. In general, the beam phase control system is designed so that it can be arbitrarily turned on and off by the central control system using timing events.

A. Experimental Setup

In the following, the general setup of the beam phase control MDE is discussed. Relevant parameters of the machine cycle are given in Table II. The ferrite-loaded cavities used for acceleration will be referred to as BE1 and BE2 (*Beschleunigungs-Einheit*, i.e., acceleration unit). Fig. 5 shows an example of their ramps for amplitude and frequency, which are used during all measurements. Furthermore, the ramp for the linear synchrotron frequency is shown. From this ramp,

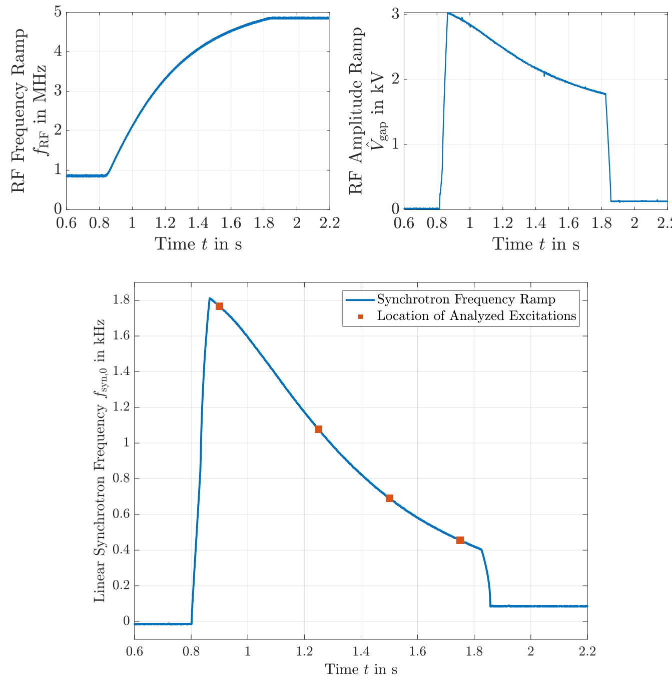

Fig. 5. Ramps for frequency (top left) and amplitude (top right) for each of the two RF cavities (i.e., maximum sum voltage of about 6 kV) as well as for the linear synchrotron frequency (bottom).

TABLE II
Parameters of the Machine Cycle for the Experiment

Date of experiment	Nov. 24th 2023
Ion species	$^{14}N^{7+}$
Number of injected particles	$\approx 5 \times 10^9 \ldots 6 \times 10^9$
Injection energy	11.362 MeV/u
Extraction energy	1000.0 MeV/u
Ramp rate	1 T/s
Harmonic number	4

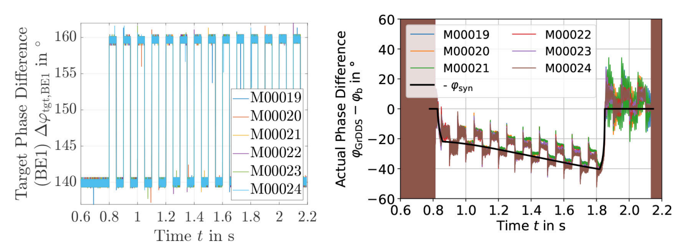

Fig. 6. Target phase for the gap voltage of BE1 (left diagram) and measured phase difference between the phase of the group DDS signal φ_{GrDDS} and the phase of the beam current φ_{b} for six repetitions of the machine cycle as well as the (negative) ramp of the synchronous phase φ_{syn} (right diagram).

the filter center frequency f_{pass} for the detection of bunch oscillations is selected and the gain K for the feedback is determined (see Section II-B). The shown actual values for the amplitude are extracted from the recorded RF signals using a sine-fitting algorithm applied to a segmented measurement of the RF gap voltage [48], [68].

In order to test the beam phase control, strong bunch oscillations were artificially induced. This was achieved by modulating the target phase of cavity BE1 with alternating steps by 20° every 50 ms along the entire duration of the machine cycle as shown in the left diagram of Fig. 6 and

TABLE III

RATIO OF THE EXTREME VALUES OF THE PHASE DIFFERENCE FOR SUBSEQUENT PERIODS AFTER EXCITATION (SEE FIG. 7). TO ACCOUNT FOR RESIDUAL OSCILLATIONS, THE SETTLED VALUES OF MINIMA/MAXIMA ARE SUBTRACTED BEFORE DIVISION. LARGER RATIOS CORRESPOND TO STRONGER DAMPING. RANGES DESCRIBE THE SPAN OF THE THREE RESPECTIVE MEASUREMENT REPETITIONS. CELLS ARE COLORED BASED ON THE MEAN VALUE SORTED INTO FOUR EQUIDISTANT INTERVALS

Time	Extrema	With BPC			Without BPC		
		$p=1$	$p=2$	$p=3$	$p=1$	$p=2$	$p=3$
0.90 s	Minima	2.67 … 3.61	1.64 … 1.86	1.62 … 2.23	1.15 … 1.35	1.27 … 1.38	1.08 … 1.29
	Maxima	2.25 … 2.71	1.46 … 2.84	1.78 … 3.54	1.17 … 1.35	1.19 … 1.52	1.25 … 1.54
1.25 s	Minima	2.25 … 2.64	1.90 … 2.09	1.22 … 1.70	1.37 … 1.68	1.41 … 2.47	1.47 … 2.25
	Maxima	2.79 … 3.01	1.58 … 2.01	1.23 … 1.95	1.29 … 1.41	1.38 … 1.92	1.55 … 1.83
1.50 s	Minima	2.45 … 2.74	2.01 … 2.12	1.40 … 1.90	1.49 … 1.68	1.58 … 1.97	1.29 … 1.65
	Maxima	2.08 … 2.56	1.49 … 1.87	1.43 … 1.51	1.44 … 1.60	1.48 … 1.77	1.24 … 1.53
1.75 s	Minima	1.66 … 1.84	1.43 … 1.56	1.52 … 3.23	1.42 … 1.87	1.64 … 2.73	1.21 … 2.41
	Maxima	1.64 … 1.78	1.40 … 1.77	1.90 … 2.13	1.29 … 1.46	1.48 … 2.64	1.72 … 2.72

marked as φ_{exci} in Fig. 1. The target phase of BE2, on the other hand, was supplied by the central control system as usual. As a consequence of each step in BE1's target phase, the synchronization control loop of the cavity quickly (in about 100 μs) shifted its gap voltage by 20° (see also, for example, [51], [62]), which is approximately equal to a non-adiabatic phase shift of the sum gap voltage of both cavities by 10°. Since the bunches have to follow such a shift in the sum gap voltage to regain their synchronous phase, oscillations were excited. Of course, for the normal operation of the synchrotron, inducing such oscillations is unwanted. The presented scheme is purely used to allow studying the reaction of the beam phase control to bunch oscillations. The right diagram in Fig. 6 displays the recorded actual phase difference $\varphi_{\text{GrDDS}} - \varphi_{\text{b}}$. It shows that this scheme indeed induced repeated oscillations of the beam phase, which are superimposed on its slowly varying value over the course of the ramp. As discussed in Section II, the phase difference is passed to the FIR filter, as shown in Fig. 6. The synchronous phase does not need to be subtracted since all slowly varying changes are disregarded by the FIR filter.

B. Dampening of Beam Phase Oscillations on the Ramp

In a first step, the functionality of the beam phase control on the ramp was demonstrated and examined. For this purpose, three repetitions of the synchrotron cycle were captured during which the beam phase control is activated (measurements 19, 20, and 21), followed by three repetitions in which the control loop was deactivated (measurements 22, 23, and 24). Fig. 7 shows the measured phase difference after excitation at four different locations along the ramp (see Fig. 6). Differences in the starting time of the ramps and the application of the excitations between cycle repetitions in the (sub-) millisecond range are manually adjusted for better comparison between graphs and figures. The differences between repetitions of the measurement with the same settings— i.e., the beam phase control being either active or inactive—are small. On the other hand, the difference between the beam phase control being active and being inactive is very noticeable. Again, it should be emphasized that the beam phase control is typically not set up to dampen preexisting oscillations as aggressively as possible (which may be at the expense of robustness). It is expected that the purposefully excited oscillations in this experiment

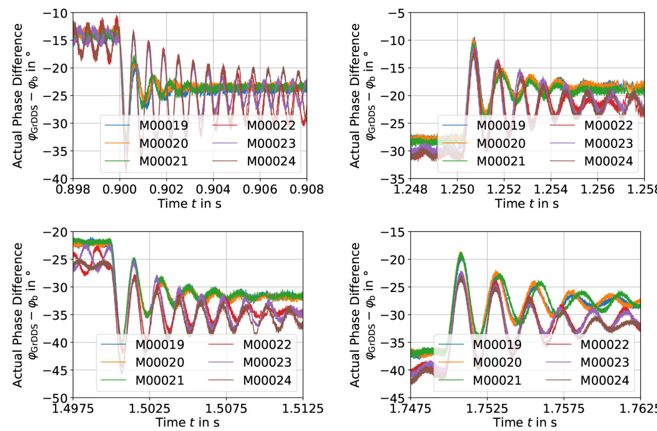

Fig. 7. Phase difference between group DDS signal φ_{GrDDS} and the beam current φ_{b} at various points in time along the acceleration ramp. It should be noted that the upper and lower diagrams have a different scaling of the time axis.

are much larger than those arising due to small errors or disruptions during normal operation. Furthermore, it is of course the primary goal of the beam phase control to dampen emerging instabilities before they can grow. When using the beam phase control, the oscillations following an excitation are less severe and decay more quickly. Any noticeable residual oscillations of the beam phase in the settled state are removed. Table III quantifies the transient decay of the beam phase oscillations. For the given results, the phase differences at the first four minima m_p and maxima M_p after each excitation are read out ($p \in \{1, 2, 3, 4\}$). Subsequently, the settled value of the minima (m_∞) or maxima (M_∞) is subtracted and the ratio for consecutive periods is calculated, i.e., $(m_p - m_\infty)/(m_{p+1} - m_\infty)$ or $(M_p - M_\infty)/(M_{p+1} - M_\infty)$, respectively. This process is repeated for each of the six measurements, which are shown in Fig. 7. It can be clearly deduced that the use of the beam phase control leads to a much improved damping during the first oscillation period, which is the most important one to prevent emittance blow-up. As expected, the overall damping is slightly less effective for lower synchrotron frequencies at the end of the acceleration ramp. From Section II-B, it can be assumed that this is due to the increasing deviations of the ratio $\chi = f_{\text{pass}}/f_{\text{syn,0}}$ below 500 Hz from the ideal value of 1 (see Fig. 3). As an example, the linear synchrotron frequency at excitation point 4 (at around 1.75 s) is about 480 Hz. From (7)

TABLE IV

OSCILLATION FREQUENCY OF THE PHASE DIFFERENCE FOR THE DIAGRAMS DISPLAYED IN FIG. 7 IN COMPARISON TO THE LINEAR SYNCHROTRON FREQUENCY CALCULATED FROM THE RF SIGNALS

Time	Observed frequency with beam phase control	Observed frequency without beam phase control	Linear synchrotron frequency from calculated ramp
0.90 s	1160 Hz…1300 Hz	1500 Hz…1610 Hz	1799 Hz…1805 Hz
1.25 s	750 Hz…840 Hz	990 Hz…1090 Hz	1095 Hz…1101 Hz
1.50 s	540 Hz…610 Hz	650 Hz…730 Hz	706 Hz…716 Hz
1.75 s	380 Hz…430 Hz	430 Hz…490 Hz	474 Hz…482 Hz

and (8), it follows that the relative error for the tuning of f_{pass} is 0% for $f_{\text{syn},0} = 500$ Hz but is already −6% for $f_{\text{syn},0} = 480$ Hz. This confirms that a non-ideal tuning is a possible reason for the observed lower damping of the feedback. However, it should also be noted that the damping of the beam phase oscillations without feedback (i.e., only due to filamentation) increases toward the end of the ramp. This also contributes to the fact that the difference between the feedback being off and on is less distinct at excitation point 4.

The oscillation frequency of the phase difference can be roughly determined from the diagrams of Fig. 7 by reading the time between extrema for the first few oscillation periods. Table IV shows the comparison of the frequency of the oscillations induced by the shown excitations for the cases with and without beam phase control. In addition, the corresponding value for the linear synchrotron frequency for the time of each excitation is given. It can be observed that the oscillation frequency without beam phase control is close to the calculated synchrotron frequency. As expected, the frequency of the coherent bunch oscillation is generally slightly lower than the linear single particle synchrotron frequency. For a bunch of finite size, some of the contained particles must occupy areas of phase space with increased revolution times (see [69] and the References therein), thus, depending on the bunch length, leading to a lower coherent bunch oscillation frequency denoted as effective synchrotron frequency in [70]. When using the beam phase control, it is notably further reduced. This is qualitatively consistent with the simplified model of a harmonic oscillator, for which the oscillation frequency decreases for increasing damping.

Analogously, this can also be observed by directly examining the FCT signal of the beam current, which is drawn in Fig. 8 as a waterfall diagram for a single excitation. Using the beam phase control, the induced oscillation of the ion bunches decays more quickly, and the original longitudinal bunch shape is essentially preserved. The results are similar for the other repetitions, bunches, and excitations.

Furthermore, the signal of the DC beam current transformer also indicates that the beam phase control helps to counteract beam losses. Corresponding measurements are shown in Fig. 9. All six repetitions start with an almost identical beam current at injection. Nevertheless, at flattop the first three repetitions—for which the beam phase control was active—all ended up with a notably higher beam current than all of the following three—for which the beam phase control was deactivated. The reason seems that without the beam phase control losses occur in the later stages of acceleration caused

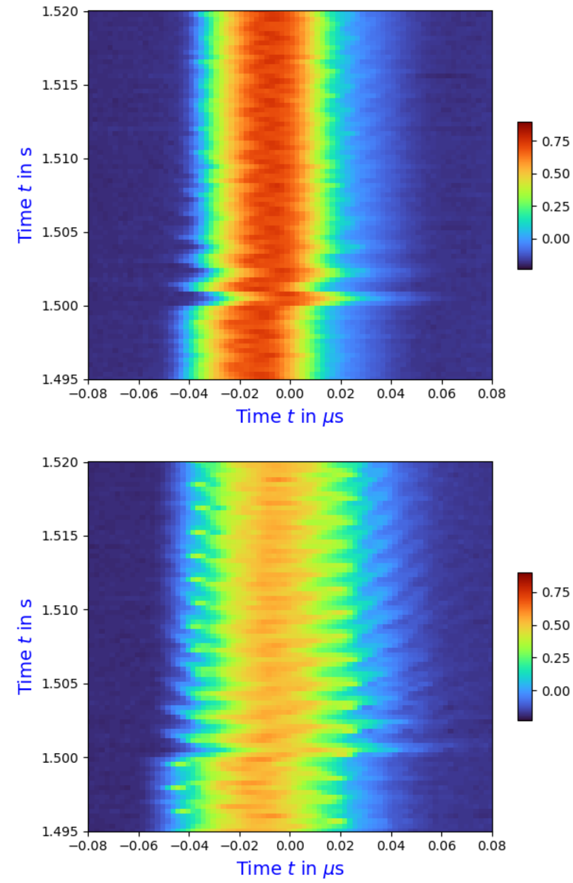

Fig. 8. Waterfall diagram of the FCT signal zoomed on one ion bunch after the excitation of the beam phase at approximately 1.5 s. Measurement 21 with beam phase control (top). Measurement 23 without beam phase control (bottom).

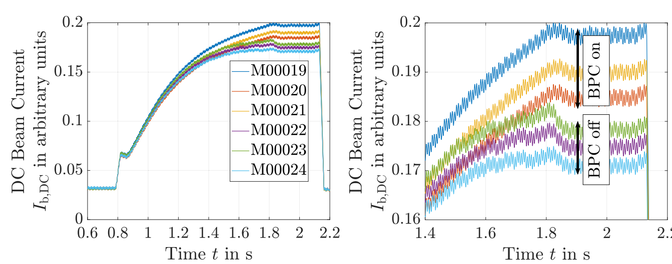

Fig. 9. DC beam current during the machine cycle for six repetitions of the measurement. The curves have been smoothed for visual clarity using a moving average of 6000 points (about 30 ms). Full cycle (left). Zoomed-in view (right).

by the continued excitation of the beam phase. Noteworthy examples can be seen when comparing measurements 21 and 23 after the excitation at 1.5 s or measurements 20 and 22 after 1.6 s.

Fig. 10 additionally visualizes this behavior by comparing the number of particles during the machine cycle (calculated from a DC beam current measurement) for measurements 21 and 23. Thus, using the beam phase control notably reduces the number of particles lost due to the applied excitations. Previous measurements without the artificial excitations showed virtually no particle loss during acceleration.

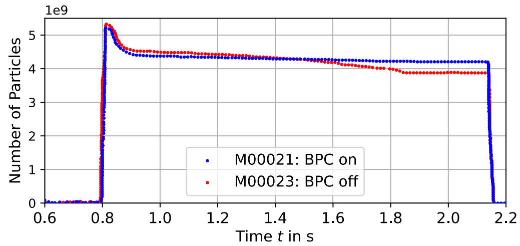

Fig. 10. Number of particles during the synchrotron cycle: measurement 21 with and measurement 23 without beam phase control. Data extracted from screenshots using [71].

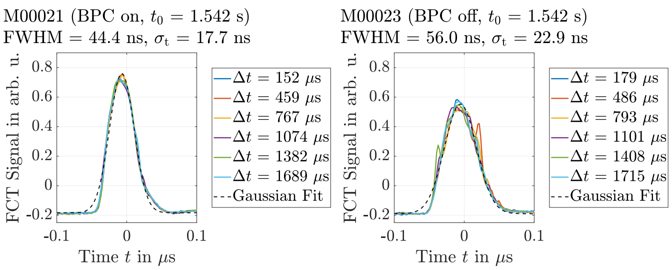

Fig. 11. Snapshots of the FCT signal for one of the four ion bunches at different points in time $t_0 + \Delta t$. Measurement 21 with the beam phase control being active (left). Measurement 23 without beam phase control (right).

Finally, Fig. 11 illustrates the short-term evolution of the shape of one of the circulating ion bunches after the previously discussed excitation applied at 1.5 s in the machine cycle. Again, measurement 21 and measurement 23 are compared. Using the beam phase control, the bunch shapes are noticeably more uniform and show only minimal variations over the displayed time interval of roughly 1.5 ms. It can be deduced that the observed beam losses can be traced back to the ongoing filamentation of the bunches due to their induced oscillations. By quickly dampening these oscillations, the beam phase control effectively prevents the filamentation of the bunches and thereby counteracts particle losses. For the sake of robustness, the full width at half maximum (FWHM) is determined from the median of the six displayed curves and the standard deviation σ_t from a Gaussian fit thereof. Without the beam phase control, the width of the bunches is increased further indicating an emittance blowup.

C. Parameter Study of the Beam Phase Control Loop

Now, it is examined how the control loop parameters influence its performance. As analyzed in Section III-B, for the applied scheme of periodic excitations, the number of particles that are lost along the ramp can be utilized as a quantitative measure for this goal. Fig. 12 shows the measured results. The particle losses occurring at the very start of acceleration (see Fig. 10) are neglected as they are caused by the injection and capture process. Repetitions of measurements with identical parameters are stacked as circles with different radii. Via changes in Δf, the filter center frequency is varied relative to the expected (linear) synchrotron frequency.

A robust optimum can be obtained for $\chi = f_{\mathrm{pass}}/f_{\mathrm{syn,0}} \approx 1$ and $K/\omega_{\mathrm{syn,0}} \approx 0.35$. As mentioned in Section II-B, this is consistent with prior analyses for operation at a constant synchrotron frequency [49], [51], [53] and is obviously confirmed here for the nested control loops of the final LLRF system. Therefore, it can be concluded that a stable and effective operation along the ramp is achieved using the scheme described in Section II-B, i.e., adjusting the filter center frequency and loop gain in accordance with the synchrotron frequency.

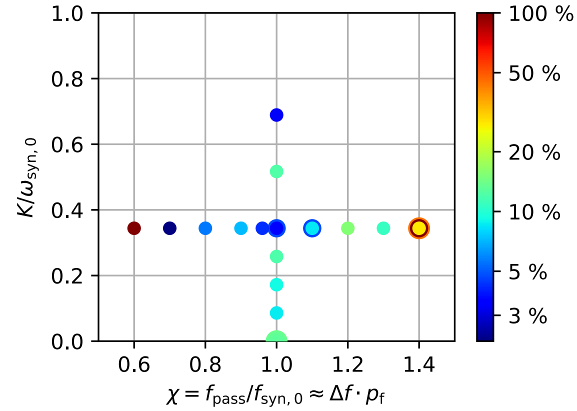

Fig. 12. Particle losses during one machine cycle as presented in Section III-A on the ramp depending on the control loop parameters.

In general, for non-ideal control loop configurations, the rate of particle losses increases along the acceleration ramp with most losses occurring during the transition to flattop as visualized in Fig. 10 for "BPC off" (which corresponds to the case of $K = 0$). This is expected for the following reasons.

1) As previously discussed in Section III-B, repeated excitations of coherent oscillations lead to filamentation of the bunches, resulting in greater losses toward the end of the ramp.
2) With the used filtering scheme presented in Section II-B, for the very low synchrotron frequencies toward the end of a machine cycle larger relative deviations in the selection of the bandpass center frequency f_{pass} are possible, thereby increasing the difficulty for detecting and counteracting bunch oscillations.
3) During the transition to flattop, the bunches naturally experience a large shift in synchronous phase which can be seen in Fig. 6.

D. Performance in a Practical Setting

The beam phase control system was used for a further beam shift at SIS18 with different machine settings. No intentional excitations (phase jumps) were used and the beam intensity was an order of magnitude higher compared to the experiment discussed first. Dipole oscillations appeared and persisted during the complete cycle, making this an ideal test case for the performance of the beam phase control during standard beam operation. This section presents the most illustrative result of the subsequent measurements.

Table V shows characteristic parameters and in Fig. 13 the ramps of the machine cycle are presented. In comparison to the cycle presented in Section III-A, the number of particles being larger by more than an order of magnitude resulted in

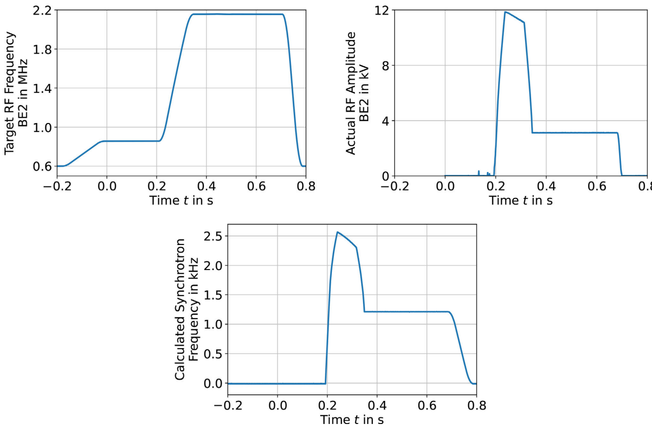

Fig. 13. Ramps for frequency (top left) and measured amplitude (top right) as well as linear synchrotron frequency (bottom) of the high-current machine cycle.

TABLE V

PARAMETERS OF THE HIGH-CURRENT MACHINE CYCLE

Date of experiment	Nov. 22nd 2023
Ion species	$^{14}N^{7+}$
Number of injected particles	$\approx 8 \times 10^{10}$
Injection energy	$11.36\,\mathrm{MeV/u}$
Extraction energy	$80\,\mathrm{MeV/u}$
Harmonic number	4

a much larger beam current, although the extraction energy is smaller. Only cavity BE2 was used for acceleration.

Fig. 14 shows waterfall diagrams of machine cycles performed with and without activated beam phase control. In the case without beam phase control (lower diagram), bunch oscillations were present during the entire machine cycle. Bunches with strong dipole oscillations also exhibited an additional quadrupole component. Notably, comparing the four different bunches shows differences both in magnitude and frequency of the respective oscillations. It can be observed that the bunches are partly oscillating out of phase. Furthermore, in contrast to the previously discussed experiment, these oscillations were not purposefully generated but arise during normal operation. It needs to be considered that the waterfall diagram was captured at 1 segment per ms, so that the displayed bunch oscillations are subject to aliasing. Analogously, Fig. 15 shows the phase difference between the group DDS signal and the beam current captured by the DSP system. Without the beam phase control, a constant oscillation of the beam phase with a frequency of about 1075 Hz at flattop was present. As shown in Section III-B, the observed oscillation frequency is slightly lower than the predicted linear synchrotron frequency, which is expected regarding the nonlinear particle motion. Using the beam phase control, this oscillation of the beam phase is almost completely removed. The corresponding waterfall diagram (top diagram in Fig. 14) underlines that all bunch oscillations during the entire machine cycle are massively reduced. This proves the practical usability of the beam phase control system.

As the remaining small dipole oscillations are out-of-phase, they are more difficult to dampen by the beam phase control system due to their diminished impact on the total beam

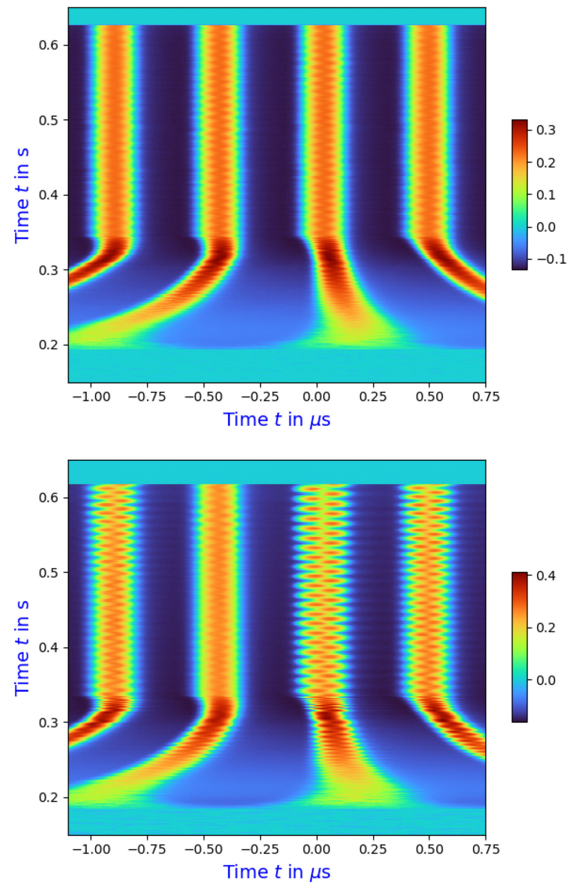

Fig. 14. Waterfall diagram of the FCT signal during the high-current machine cycle. With beam phase control (top). Without beam phase control. Notice the difference in color mappings (bottom).

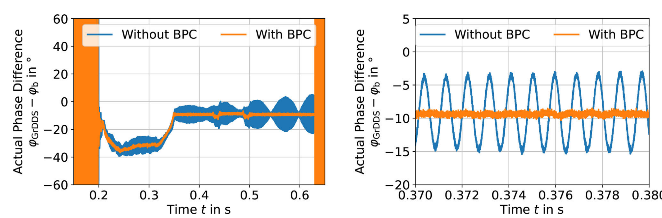

Fig. 15. Phase difference between group DDS signal φ_{GrDDS} and the beam current φ_{b} with and without beam phase control. Full cycle (left). Zoom onto flattop (right).

phase. The bunch-by-bunch longitudinal feedback system being developed for SIS100 at FAIR will expand the functionality to dampen each bunch's dipole oscillation individually, as well as also higher order modes [72], [73].

IV. CONCLUSION

The performance of the GSI/FAIR beam phase control system was evaluated in a dedicated MDE as well as during a shift using standard machine settings and a higher beam intensity. It was shown that the system is able to damp coherent dipole oscillations sufficiently fast for various oscillation frequencies during the acceleration cycle. Although the final LLRF topology includes nested control loops, the optimal parameters of the system are similar to those obtained in the original analysis that did not consider this aspect or the variable filter. Improvements for standard beam operation are still possible. For example, enabling a non-equidistant distribution of the filter center frequencies with a finer resolution at lower synchrotron frequencies would improve the automatic tuning accuracy. The presented topology of the beam phase control will also be used for the SIS100 synchrotron in construction at FAIR.

Acknowledgment

This work would not have been possible without the support of many colleagues and groups at GSI (RRF, SYS, BEA, ACO, and OPE). Furthermore, the authors wish to express their thanks to the many colleagues of the Ring RF Systems Department, GSI and the Accelerator Technology Group, TU Darmstadt who have contributed to the realization of the feedback system as well as to preparing and conducting the experiments. In particular, special thanks are expressed to S. Schäfer, C. Thielmann, and G. Thomin.

References

[1] A. V. Dolinskii, H. Eickhoff, and B. J. Franczak, "The synchrotron of the dedicated ion beam facility for cancer therapy, proposed for the clinic in Heidelberg," in *Proc. EPAC*, Vienna, Austria, 2000, pp. 2509–2511.

[2] D. Ondreka and U. Weinrich, "The Heidelberg ion therapy (HIT) accelerator coming into operation," in *Proc. EPAC*, Genoa, Italy, 2008, pp. 979–981.

[3] A. Peters, "The accelerator facility of the Heidelberg ion-beam therapy centre (HIT)," in *Challenges and Goals for Accelerators in the XII Century*, 1st ed., Singapore: World Scientific, 2021, ch. 4, pp. 801–812. [Online]. Available: https://www.worldscientific.com/worldscibooks/10.1142/8635

[4] C. Schmitzer et al., "MedAustron synchrotron RF commissioning for medical proton beams," in *Proc. IPAC*, 2016, pp. 844–846.

[5] M. Benedikt, "MedAustron: The Austrian ion therapy facility," in *Challenges and Goals for Accelerators in the XII Century*, 1st ed., Singapore: World Scientific, 2021, ch. 4, pp. 813–824. [Online]. Available: https://www.worldscientific.com/worldscibooks/10.1142/8635

[6] M. T. F. Pivi, "The MedAustron particle therapy accelerator facility," *Health Technol.*, vol. 14, no. 5, pp. 919–928, Apr. 2024, doi: 10.1007/s12553-024-00840-z.

[7] M. Chanel, "LEIR: The low energy ion ring at CERN," *Nucl. Instrum. Methods Phys. Res. A, Accel. Spectrom. Detect. Assoc. Equip.*, vol. 532, nos. 1–2, pp. 137–143, Oct. 2004, doi: 10.1016/j.nima.2004.06.040.

[8] M. E. Angoletta et al., "Beam tests of a new digital beam control system for the CERN LEIR accelerator," in *Proc. Part. Accel. Conf.*, Knoxville, TN, USA, 2005, pp. 1649–1651.

[9] M. E. Angoletta et al., "CERN's LEIR digital LLRF: System overview and operational experience," in *Proc. IPAC*, Kyoto, Japan, 2010, pp. 1464–1466.

[10] M. E. Angoletta, A. Butterworth, A. Findlay, and S. Hancock, "Operational experience with the new LEIR digital low-level RF system," CERN, Geneve, Switzerland, Tech. Rep. CERN-ATS-Note-2010-054 TECH, 2025. [Online]. Available: https://cds.cern.ch/record/1313731/files/CERN-ATS-Note-2010-054-tech.pdf

[11] A. S. Hernandez, D. Moreno, H. Bartosik, N. Biancacci, S. Hirlander, and A. Huschauer, "Space charge studies on LEIR," *J. Phys., Conf. Ser.*, vol. 1067, no. 6, 2018, Art. no. 062020.

[12] S. Albright et al., "Review of LEIR operation in 2018," CERN, Geneva, Switzerland, Tech. Rep. CERN-ACC-Note-2020-0023, 2025. [Online]. Available: https://cds.cern.ch/record/2715365/files/CERN-ACC-NOTE-2020-0023.pdf

[13] M. E. Angoletta et al., "Achievements and new challenges for CERN's digital LLRF family," 2019, *arXiv:1910.06643*.

[14] R. A. Fernández, "Introduction to CERN and its accelerator complex," in *Proc. JUAS*, Geneva, Switzerland, 2024, pp. 1903–1923.

[15] B. Franczak, "SIS parameter list," GSI Helmholtzzentrum für Schwerionenforschung GmbH, Darmstadt, Germany, Tech. Rep. GSI-SIS-TN/87-13, 2025. [Online]. Available: https://www.gsi.de/fileadmin/PSchwab/Dokumentationen_Berichte/Beschleunigeranlage/SIS18/sis18_parameterliste.pdf

[16] D. Ondreka, C. Dimopoulou, H. C. Hüther, H. Liebermann, J. Stadlmann, and R. J. Steinhagen, "Recommissioning of SIS18 after FAIR upgrades," in *Proc. IPAC*, Melbourne, VIC, Australia, 2019, pp. 932–935.

[17] P. J. Spiller, "Status of the FAIR synchrotron projects SIS18 upgrade and SIS100," in *Proc. IPAC*, 2014, pp. 1857–1860.

[18] H. Liebermann and D. Ondreka, "FAIR and GSI reference cycles for SIS18, "FAIR and GSI reference cycles for SIS18," GSI Helmholtzzentrum für Schwerionenforschung GmbH, Darmstadt, Germany, Tech. Rep., 2025. [Online]. Available: https://www.gsi.de/fileadmin/PSchwab/Dokumentationen_Berichte/Beschleunigeranlage/SIS18/FAIR_GSI_Reference_Cycles_SIS18_version_1.2.pdf

[19] E. Cullerton, B. Schupbach, B. Pellico, B. Chase, P. Varghese, and D. Klepec, "Fermilab PIP-II booster LLRF upgrade," Fermi National Accelerator Laboratory, Batavia, IL, USA, Tech. Rep. FERMILAB-CONF-19-530-AD-PIP2, 2025. [Online]. Available: https://www.osti.gov/biblio/1605575

[20] C. M. Bhat et al., "Recent improvements in the beam capture at fermilab booster for high intensity operation," in *Proc. ICFA ABDW*, Batavia, IL, USA, 2021, pp. 23–26.

[21] F. Tamura, Y. Sugiyama, M. Yoshii, and M. Ryoshi, "Development of next-generation LLRF control system for J-PARC rapid cycling synchrotron," *IEEE Trans. Nucl. Sci.*, vol. 66, no. 7, pp. 1242–1248, Jul. 2019, doi: 10.1109/TNS.2019.2899358.

[22] F. Tamura et al., "Commissioning of the next-generation LLRF control system for the rapid cycling synchrotron of the Japan proton accelerator research complex," *Nucl. Instrum. Methods Phys. Res. A, Accel. Spectrom. Detect. Assoc. Equip.*, vol. 999, May 2021, Art. no. 165211, doi: 10.1016/j.nima.2021.165211.

[23] F. Tamura et al., "Multiharmonic vector Rf voltage control for wideband cavities driven by vacuum tube amplifiers in a rapid cycling synchrotron," *Phys. Rev. Accel. Beams*, vol. 22, no. 9, pp. 092001-1–092001-22, Sep. 2019, doi: 10.1103/physrevaccelbeams.22.092001.

[24] *Booster Design Manual*, Accelerator Development Department, Upton,, NY, USA, 1988.

[25] C. J. Gardner, "FY10 parameters for the injection, acceleration, and extraction of gold ions in Booster, AGS, and RHIC," BNL, Upton, NY, USA, Tech. Rep. BNL-93899-2010-IR, 2010.

[26] S. Y. Zhang and L. A. Ahrens, "Booster gold beam injection efficiency and beam loss," in *Proc. EPAC*, Stockholm, Sweden, 1998, pp. 2149–2151.

[27] M. E. Angoletta et al., "CERN's PS booster LLRF renovation: Plans and initial beam tests," in *Proc. IPAC*, Kyotot, Japan, 2010, pp. 1461–1463.

[28] C. Carter, J. Fopma, G. Gelato, L. Magnani, P. Odier, and K. Schindl. *Adapting the CERN PS Booster To Oxygen Acceleration*. Accessed: May 15, 2025. [Online]. Available: https://cds.cern.ch/record/2835705/files/CERN-PS-BR-87-35.pdf

[29] F. Blas, P. Bossard, R. Cappi, G. Cyvoct, R. Garoby, and G. Gelato, "Acceleration of lead ions in the CERN PS Booster and the CERN PS," in *Proc. PAC*, Dallas, TX, USA, 1995, pp. 423–425.

[30] K. Hanke, "Past and present operation of the CERN PS booster," *Int. J. Mod. Phys. A*, vol. 28, no. 13, May 2013, Art. no. 1330019.

[31] M. M. Paoluzzi et al., "Design of the new wideband RF system for the CERN PS booster," in *Proc. IPAC*, 2016, pp. 441–443.

[32] F. Pedersen and F. Sacherer, "Theory and performance of the longitudinal active damping system for the CERN PS booster," *IEEE Trans. Nucl. Sci.*, vol. NC-24, no. 3, pp. 1396–1398, Jun. 1977, doi: 10.1109/TNS.1977.4328956.

[33] D. Boussard, "Control of cavities with high beam loading," *IEEE Trans. Nuc. Sci.*, vol. NC-32, no. 5, pp. 1852–1856, May 1985.

[34] S. Koscielniak, "RF system aspects of longitudinal beam control (in the low current regime)," *AIP Conf. Proc.*, vol. 249, no. 1, pp. 89–149, Mar. 1992.

[35] F. Pedersen, "RF cavity feedback," presented at the Conf. B Factories, 2025. [Online]. Available: https://cds.cern.ch/record/244817/files/CM-P00059367.pdf

[36] R. Garoby, "Low Level RF and feedback," in *Frontiers of Accelerator Technology*, 1st ed., Singapore: World Scientific, 1999, pp. 455–489.

[37] D. Boussard, "Design of a ring RF system," in *CERN—Rutherford Accelerator School: RF Engineering for Particle Accelerators*. European Organization forNuclear Research (CERN): Oxford, U.K., 1991, pp. 474–500.

[38] D. Barrientos, S. Albright, M. E. Angoletta, A. Findlay, M. Jaussi, and J. Molendijk, "A new beam loading compensation and blowup control system using multi-harmonic digital feedback loops in the CERN proton synchrotron booster," in *Proc. IPAC*, Bangkok, Thailand, 2022, pp. 907–910.

[39] F. Severino, M. Harvey, T. Hayes, G. Narayan, and K. S. Smith, "Distributed feedback loop implementation in the RHIC low level RF platform," in *Proc. ICALEPCS*, San Francisco, CA, USA, 2013, pp. 1501–1504.

[40] M. E. Angoletta, S. Albright, A. Findlay, M. Jaussi, J. Molendijk, and N. Pittet, "Upgrade of CERN's PSB digital low-level RF system," in *Proc. IPAC*, Melbourne, VIC, Australia, 2019, pp. 3958–3961.

[41] S. Albright, M. E. Angoletta, D. Barrientos, A. Findlay, M. Jaussi, and J. Molendijk, "Commissioning the new LLRF system of the CERN PS booster," in *Proc. IPAC*, Bangkok, Thailand, 2022, pp. 2060–2063.

[42] D. Wildman, "Transient beam loading compensation in the fermilab main ring," *IEEE Trans. Nucl. Sci.*, vol. NC-32, no. 5, pp. 2150–2152, Oct. 1985, doi: 10.1109/TNS.1985.4333845.

[43] F. Tamura et al., "Multiharmonic RF feedforward system for beam loading compensation in wide-band cavities of a rapid cycling synchrotron," *Phys. Rev. Special Topics-Accel. Beams*, vol. 14, no. 5, pp. 051004-1–051004-15, May 2011, doi: 10.1103/physrevstab.14.051004.

[44] A. Schnase et al., "Control loops for the J-PARC RCS digital low-level RF control," in *Proc. Part. Accel. Conf.*, Knoxville, TN, USA, 2005, pp. 1063–1065, doi: 10.1109/pac.2005.1590659.

[45] J. M. Brennan et al., "RF beam control system for the brookhaven relativistic heavy ion collider, RHIC," in *Proc. EPAC*, Stockholm, Sweden, 1998, pp. 1705–1707.

[46] E. Onillon and J. M. Brennan, "The new BNL AGS phase, radial and synchronization loops," in *Proc. EPAC*, Barcelona, Spain, 1996, pp. 1842–1844.

[47] B. Zipfel et al., "Experimental results on longitudinal RF beam phase feedback in the heavy-ion synchrotron SIS18," in *Proc. IPAC*, 2024, pp. 3329–3332.

[48] A. Andreev, D. Lens, and H. Klingbeil, "A calibration system for hadron synchrotrons with a large frequency swing," *Nucl. Instrum. Methods Phys. Res. A, Accel. Spectrom. Detect. Assoc. Equip.*, vol. 1053, Aug. 2023, Art. no. 168382, doi: 10.1016/j.nima.2023.168382.

[49] J. Grieser et al., "A digital beam-phase control system for a heavy-ion synchrotron with a dual-harmonic cavity system," *IEEE Trans. Nucl. Sci.*, vol. 61, no. 6, pp. 3584–3591, Dec. 2014, doi: 10.1109/TNS.2014.2367911.

[50] H. Klingbeil, "A fast DSP-based phase-detector for closed-loop RF control in synchrotrons," *IEEE Trans. Instrum. Meas.*, vol. 54, no. 3, pp. 1209–1213, Jun. 2005, doi: 10.1109/TIM.2005.847138.

[51] H. Klingbeil, B. Zipfel, M. Kumm, and P. Moritz, "A digital beam-phase control system for heavy-ion synchrotrons," *IEEE Trans. Nucl. Sci.*, vol. 54, no. 6, pp. 2604–2610, Dec. 2007, doi: 10.1109/TNS.2007.909666.

[52] F. J. Sacherer, "A longitudinal stability criterion for bunched beams," *IEEE Trans. Nucl. Sci.*, vol. NC-20, no. 3, pp. 825–829, Jun. 1973, doi: 10.1109/TNS.1973.4327254.

[53] H. Klingbeil, D. Lens, M. Mehler, and B. Zipfel, "Modeling longitudinal oscillations of bunched beams in synchrotrons," 2010, *arXiv:1011.3957*.

[54] M. Bousonville and J. Rausch, "Universal picosecond timing system for the facility for antiproton and ion research," *Phys. Rev. Special Topics-Accel. Beams*, vol. 12, no. 4, pp. 042801-1–042801-10, Apr. 2009, doi: 10.1103/physrevstab.12.042801.

[55] M. Bousonville and J. Rausch, "Reference signal generation with direct digital synthesis for FAIR," in *Proc. HIAT*, Venice, Italy, 2009, pp. 218–222.

[56] J. Serrano et al., "The White Rabbit project," in *Proc. ICALEPCS*, Kobe, Japan, 2009, pp. 93–95.

[57] M. Lipinski, T. Włostowski, J. Serrano, and P. Alvarez, "White rabbit: A PTP application for robust sub-nanosecond synchronization," in *Proc. IEEE Int. Symp. Precis. Clock Synchronization Meas., Control Commun.*, Sep. 2011, pp. 25–30, doi: 10.1109/ISPCS.2011.6070148.

[58] J. Serrano et al., "The White Rabbit project," in *Proc. IBIC*, Oxford, U.K., 2013, pp. 936–942.

[59] T. Włostowski et al., "Trigger and RF distribution using White Rabbit," in *Proc. ICALEPCS*, 2015, pp. 619–623.

[60] D. Beck et al., "The new White Rabbit based timing system for the FAIR facility," in *Proc. PCaPAC*, Kolkata, India, 2012, pp. 242–244.

[61] C. Prados et al., "FAIR timing system developments based on White Rabbit," in *Proc. ICALEPCS*, San Francisco, CA, USA, 2013, pp. 1288–1291.

[62] H. Klingbeil, U. Laier, K.-P. Ningel, S. Schäfer, C. Thielmann, and B. Zipfel, "New digital low-level RF system for heavy-ion synchrotrons," *Phys. Rev. Special Topics-Accel. Beams*, vol. 14, no. 10, Oct. 2011, Art. no. 102802, doi: 10.1103/physrevstab.14.102802.

[63] A. Andreev, H. Klingbeil, and D. Lens, "Phase calibration of synchrotron RF signals," in *Proc. IPAC*, Copenhagen, Denmark, 2017, pp. 3945–3947.

[64] D. Lens et al., "Bunch merging and compression: Recent progress with RF and LLRF systems for FAIR," in *Proc. HIAT*, Darmstadt, Germany, 2022, pp. 67–71.

[65] M. Hoffmann et al., "The longitudinal coupled bunch feedback for HERA-p," in *Proc. EPAC*, 2006, pp. 2985–2987.

[66] A. Guntoro, P. Zipf, O. Soffke, H. Klingbeil, M. Kumm, and M. Glesner, "Implementation of realtime and highspeed phase detector on FPGA," in *Reconfigurable Computing: Architectures Applications*. Berlin, Germany: Springer, 2006, pp. 1–11.

[67] S. Pongyupinpanich, "Optimal design of fixed-point and floating-point arithmetic units for scientific applications," Ph.D. dissertation, Technische Universität Darmstadt, Darmstadt, Germany, 2012.

[68] D. Lens and H. Klingbeil, "STARFISH-PY: A versatile toolchain analysis of synchrotron RF system's data," presented at the Workshop, 2017. [Online]. Available: https://public.cells.es/workshops/www.llrf2017.org/pdf/Posters/P-40.pdf

[69] J. Grieser, D. Lens, H. Klingbeil, and J. Adamy, "A method to obtain the frequency of the longitudinal dipole oscillation for modeling and control in synchrotrons with single or double harmonic RF systems," in *Proc. IPAC*, New Orleans, LA, USA, 2012, pp. 2846–2848.

[70] D. Lens and H. Klingbeil, "Stability of longitudinal bunch length feedback for heavy-ion synchrotrons," *Phys. Rev. Special Topics - Accel. Beams*, vol. 16, no. 3, pp. 032801-1–032801-13, Mar. 2013, doi: 10.1103/physrevstab.16.032801.

[71] A. Rohatgi. (2014). *WebPlotDigitizer*. [Online]. Available: https://web.eecs.utk.edu/

[72] K. Groß et al., "Bunch-by-bunch longitudinal RF feedback for beam stabilization at FAIR," in *Proc. IPAC*, Richmond, VA, USA, 2015, pp. 820–822.

[73] M. Hardieck et al., "Damping of quadrupole oscillations with bunch-by-bunch longitudinal RF feedback for FAIR," in *Proc. IPAC*, Taipei, Taiwan, 2025, pp. 2976–2979.